Hindawi
Geofluids
Volume 2021, Article ID 6690218, 15 pages
https://doi.org/10.1155/2021/6690218

Research Article

Analytical Solutions for Gas-Water Two-Phase Flow in Multiseam Coalbed Methane Production

Xiaoji Shang,[1] Zhizhen Zhang,[1,2] Yixin Niu,[1] Xiao Yang,[1] and Feng Gao[1]

[1]*State Key Laboratory of Geomechanics and Deep Underground Engineering, School of Mechanics and Civil Engineering, China University of Mining and Technology, Xuzhou 221116, China*
[2]*State Key Laboratory of Coal Mine Safety Technology, CCTEG Shenyang Research Institute, Shenyang 110016, China*

Correspondence should be addressed to Zhizhen Zhang; zzzhang@cumt.edu.cn

Received 23 December 2020; Revised 21 January 2021; Accepted 28 January 2021; Published 16 February 2021

Academic Editor: Jiehao Wang

Multiseam coalbed methane (CBM) exploitation can not only reduce single-well investment but also increase the length of service of the well and significantly enhance the CBM economic recovery of the entire basin. To compare with and further to guide the actual project of CBM production, this study proposed a conceptual gas-water two-phase separate flow model for single coal seam considering the solubility of gas. This mathematical model was solved analytically by separation of variables and verified through history matching of the production data from the No. 3 seam of 1# test well of Jincheng and then applied to investigate the effect of gas solubility on the gas pressure. Furthermore, based on the coupled two-phase separate flow model of single seam, another two-phase separate flow model for the development of multicoal seam development was established. Similarly, the analytical solution of this model for multicoal seam layers was matched with the in situ data of TS-1 well of Liupanshui coal mine. It is found that the height difference and pressure difference between the two seams play key roles in the multiseam CBM development comprehensively.

1. Introduction

To improve vertical well coalbed methane (CBM) production, a great amount of well drainage control methods have been researched, such as vertical drainage of single seam layer, multiseam fracturing drainage of multicoal seam layers, and single-seam fracturing drainage of multicoal seam layers [1]. Through investigation of the multiseam CBM exploitation in Powder River Basin, the U.S. Department of Energy [2] has found that multiseam CBM exploitation can not only reduce single-well investment but also increase the length of service of the well and significantly enhance the CBM economic recovery of the entire basin [3]. Moreover, it is found that some wells adopting multiseam CBM exploitation have been working for more than 10 years in the earlier well group in the Panzhuang block of the southern Qinshui Basin, with the gas production remaining around 1000 m^3/d [4]. Thus, the effective development of multicoal seam layers will be helpful to obtain high yield in vertical CBM well production [4, 5].

Based on multicoal seam development, a variety of factors which can affect mining such as burial depth, coal thickness, gas content, porosity, permeability, structural setting, and damage mechanism of upper exposed producing layers have been studied [6–10]. Besides, in the technical perspective, several kinds of technology such as well test analysis, numerical simulation, and physical simulation have been applied to the development of multicoal seam [1, 11]. For instance, after the comparison between the theory and the field data from coal reservoir in southern Qinshui Basin, China, Li and Li [1] put forward that the main controlling factors influencing the multicoal seam development consist of the height of the critical production gas, the grades of reservoir pressure, the difference of ability of supply for liquid, and the permeability; in the aspect of numerical simulation, the laws of the geological mining factors to the upper and lower pillar's stability in multicoal seam strip mining were studied by FLAC3D and the function relation between the stress increasing coefficient of upper and lower pillars with the mining depth, mining widths, interlayer spacing, mining

thickness, property of interstratified rock, and the spatial relationship was obtained [11].

In order to closely simulate and further to guide the practical production of CBM wells, the modeling of multicoal seam development has become the research emphasis naturally. To select favorable regions for multiseam CBM exploitation, Zhang et al. [3] have conducted a multiobjective fuzzy matter-element model to evaluate the potential of multiseam CBM exploitation in the study area based on the correlation analysis. On the other hand, in general, pore fractures of low-rank coal reservoirs are filled with water, especially in a shallow burial depth of 1000 m [12]; thus, the study of CBM exploitation process is actually the process of two-phase flow, on which many scholars have already conducted large amount of researches [13–15]. Ibrahim and Nasr-El-Din [14] have developed an analytical model for saturated CBM reservoirs where two-phase flow occurs from the start of production, and the model can be used as a prediction or a history matching tool for CBM performance. Clarkson and McGovern [16] developed a model for simulating single-phase flow of water above desorption pressure and two-phase flow of gas and water below desorption pressure, but effects of transient flow were ignored. As a supplement, using a revised DDA model, the model of transition from single-phase to multiphase flow during transient flow for CBM reservoirs has been conducted [13]. Due to the difficulty of obtaining the analytical solution, numerical simulation is always adopted to solve the model founded in the study of two-phase flow; for example, Ziarani et al. [17] have investigated the effect of sorption time on CBM recovery through numerical simulation. However, there is almost no mathematical model focused on the relationship of the fluid pressure, production rate and mining time, mining distance on the development of multiseam layers at two-phase flow stage, not to mention the analytical solution of the fluid pressure and velocity, and so on.

It is generally accepted that CBM mainly exists in coal seam in adsorbed state, but more and more studies reveal that dissolved gas should not be ignored [18, 19]. Based on this conclusion, lots of experiments for methane solubility are conducted [12, 20]. Samples taken from Hailar Basin of Xinjiang, China, were physically simulated of dissolved methane content [12]. The experimental results indicate that the solubility of methane is influenced by temperature, pressure, coal reservoir water salinity, etc. But few coupling seepage models considering the solubility factor are established and discussed in theoretical research actually.

This paper proposes a two-phase separate flow model for the mining of multicoal seam layers. Firstly, considering the solubility of gas, a two-phase separate flow model of single seam is proposed for the multiphysical process. Secondly, this coupled mathematical model is analytically solved by separation of variables and applied to compare with the field data of the No. 3 seam of 1# test well of Jincheng, Shanxi, for the verification of model accuracy. Thirdly, the impacts of gas solubility on the gas pressure are analyzed. Furthermore, based on the coupled two-phase separate flow model of single seam, another coupled mathematical model of two-phase separate flow for the development of multicoal seam layers is established. Similarly, the analytical solutions of this model for multicoal seam layers is matched with the field data of TS-1 well of Liupanshui coal mine, China [10]. Finally, the impact of interlayer difference on the development of multicoal seam layers is demonstrated.

2. Gas-Water Two-Phase Separate Flow Model for Single-Seam CBM Development

Before the establishment of the two-phase flow model, assume that the gas and water two-phase flows are two completely separate fluids with different velocities and properties for the convenience of obtaining the analytical solutions. However, the gas solubility in water is considered in the following models.

2.1. Gas-Water Flow Continuity Equations. In the following fluid continuity equations at the two-phase flow stage, subscripts g and w are used to represent the gas phase and water phase, respectively.

The continuity equation for gas is

$$\frac{\partial}{\partial t}\left[\phi\left(R_{sw}s_w\rho_w + s_g\rho_g\right)\right] - \nabla\cdot\left[\rho_g \boldsymbol{V}_g + R_{sw}\rho_w \boldsymbol{V}_w\right] = \rho_g q_g. \tag{1}$$

The continuity equation for water is

$$\frac{\partial}{\partial t}(\phi\rho_w s_w) - \nabla\cdot(\rho_w \boldsymbol{V}_w) = \rho_w q_w, \tag{2}$$

where ϕ is the coal porosity and R_{sw} is the gas solubility in water. ρ_w is the density of water and ρ_g is the density of gas under formation conditions. V_g is the velocity of gas and V_w is the velocity of water. q_g and q_w denote the fluid strength of gas and water, respectively. ∇ is the Hamiltonian operator. s_g and s_w are the saturations of gas and water, respectively, and the pores are fully saturated by gas and water:

$$s_g + s_w = 1. \tag{3}$$

2.2. Gas-Water Flow Motion Equations. The gas-water coupled seepage equations of motion are [21]

$$\phi s_w(V_w - V_s) = -\frac{kk_{rw}}{\mu_w}(\nabla p_w - \rho_w g\nabla H), \tag{4}$$

$$\phi s_g\left(V_g - V_s\right) = -\frac{kk_{rg}}{\mu_g}\left(\nabla p_g - \rho_g g\nabla H\right), \tag{5}$$

where V_w and V_g are the absolute velocities of water and gas, respectively. V_s is the velocity of the coal solid. k is the absolute permeability of porous media. k_{rw} and k_{rg} are the relative permeabilities of water and gas, respectively. μ_w and μ_g are the viscosities of water and gas, respectively. p_w and p_g are the pore pressures of water and gas within porous media,

respectively. g is the gravity acceleration, and H refers to the vertical elevation.

According to Equations (1)–(4), ignoring the second-order phase, the governing equations of the gas-water two-phase flow are obtained.

For the water phase,

$$\left(\frac{kk_{\mathrm{rw}}}{\mu_{\mathrm{w}}\phi s_{\mathrm{w}}}\right)\nabla^2 p_{\mathrm{w}} = \mathrm{div}\ V_{\mathrm{s}} + \nabla\cdot(\rho_{\mathrm{w}} g\nabla H) + q_{\mathrm{w}} - \frac{\partial}{\partial t}(\phi s_{\mathrm{w}}). \tag{6}$$

For the gas phase,

$$\frac{1}{k}\left\{\mathrm{div}\ V_{\mathrm{s}} + \frac{\partial}{\partial t}\left[\phi\left(R_{\mathrm{sw}}s_{\mathrm{w}}\rho_{\mathrm{w}} + s_{\mathrm{g}}\rho_{\mathrm{g}}\right)\right]\right\} - \nabla \cdot \left[\left(\frac{k_{\mathrm{rg}}\rho_{\mathrm{g}}}{\mu_{\mathrm{g}}} + \frac{k_{\mathrm{rw}}R_{\mathrm{sw}}\rho_{\mathrm{w}}}{\mu_{\mathrm{w}}}\right)\nabla p_{\mathrm{g}}\right] = q_{\mathrm{g}}\rho_{\mathrm{g}}, \tag{7}$$

where

$$\mathrm{div}\ V_{\mathrm{s}} = \frac{\partial\theta}{\partial t}. \tag{8}$$

θ is the volumetric strain of the coal solid.

2.3. Deformation Field Equations of Coalbed. According to the theory of elasticity, the coalbed maintains the force balance during CBM mining, and the differential equation of equilibrium is

$$\sigma_{ij,j} + f_i = 0, \tag{9}$$

where σ_{ij} is the total stress tensor and f_i is the body force tensor.

Through the principle of effective stress, the relationship between the total stress tensor σ_{ij} and the effective stress tensor $\sigma_{ij}{}'$ can be written as

$$\sigma_{ij} = \sigma_{ij}{}' - p\delta_{ij}, \tag{10}$$

where $\sigma_{ij}{}'$ is the effective stress tensor. p denotes the pore pressure of coalbed. δ_{ij} is the Kronecker function, and it is given by

$$\delta_{ij} = \begin{cases} 1, & i = j, \\ 0, & i \neq j. \end{cases} \tag{11}$$

As described above, the coalbed experiences elastic deformation in the CBM mining process; thus, the generalized Hooke law can be used to characterize the stress-strain relationship of the coal.

$$\sigma_{ij}{}' = 2G\varepsilon_{ij} + \lambda\theta\delta_{ij} + (1-\alpha)p\delta_{ij}, \tag{12}$$

where ε_{ij} is the strain tensor, α is the Biot coefficient. G is the shear modulus of elasticity, and λ is the lame constant, and they can be written as

$$G = \frac{E}{2(1+\nu)}, \qquad \lambda = \frac{E\nu}{(1+\nu)(1-2\nu)}, \tag{13}$$

where E is the modulus of elasticity and ν is the Poisson ratio.

Suppose the coal solid produced only small deformation in the CBM mining process, the following equation can be obtained through the continuity in the deformation process as

$$\varepsilon_{ij} = \frac{1}{2}\left(u_{i,j} + u_{j,i}\right), \tag{14}$$

where u_i and u_j are the displacement components of coal solid.

From Equation (14), we can obtain

$$\theta = \nabla\cdot\mathbf{u}, \tag{15}$$

where $\mathbf{u}$ is the displacement vector.

Combined with Equations (10)–(19), the governing equations are simplified into

$$(2G+\lambda)\nabla\theta + f = \alpha\nabla p. \tag{16}$$

2.4. Fluid Pressure Model at Two-Phase Flow Stage. Combined with Equations (7), (6), and (16), the fluid pressure model in gas-water two-phase flow becomes

$$\mathrm{(I)}\begin{cases} \left(\dfrac{kk_{\mathrm{rg}}\rho_{\mathrm{g}}}{\mu_{\mathrm{g}}} + \dfrac{kk_{\mathrm{rw}}R_{\mathrm{sw}}\rho_{\mathrm{w}}}{\mu_{\mathrm{w}}}\right)\nabla^2 p_{\mathrm{g}} = \dfrac{\partial}{\partial t}\left[\phi\left(R_{\mathrm{sw}}s_{\mathrm{w}}\rho_{\mathrm{w}} + s_{\mathrm{g}}\rho_{\mathrm{g}}\right) + \dfrac{\alpha}{\lambda+2G}p_{\mathrm{g}}\right] + \mathrm{div}\ V_{\mathrm{s}} + q_{\mathrm{g}}\rho_{\mathrm{g}}, \\ \left(\dfrac{kk_{\mathrm{rw}}}{\mu_{\mathrm{w}}\phi s_{\mathrm{w}}}\right)\nabla^2 p_{\mathrm{w}} = \mathrm{div}\ V_{\mathrm{s}} + \nabla\cdot(\rho_{\mathrm{w}} g\nabla H) + q_{\mathrm{w}} - \dfrac{\partial}{\partial t}(\phi s_{\mathrm{w}}), \\ (2G+\lambda)\nabla\theta + f = \alpha\nabla p \end{cases} \tag{17}$$

This model can be further simplified into

$$(\mathrm{II})\begin{cases}\left(\dfrac{kk_{\mathrm{rg}}\rho_{\mathrm{g}}}{\mu_{\mathrm{g}}}+\dfrac{kk_{\mathrm{rw}}R_{\mathrm{sw}}\rho_{\mathrm{w}}}{\mu_{\mathrm{w}}}\right)\nabla^2 p_{\mathrm{g}}=\dfrac{\partial}{\partial t}\left[\phi\left(R_{\mathrm{sw}}s_{\mathrm{w}}\rho_{\mathrm{w}}+s_{\mathrm{g}}\rho_{\mathrm{g}}\right)\right]+\dfrac{\alpha}{\lambda+2G}\dfrac{\partial}{\partial t}p_{\mathrm{g}}+q_{\mathrm{g}}\rho_{\mathrm{g}},\\ \left(\dfrac{kk_{\mathrm{rw}}}{\mu_{\mathrm{w}}\phi s_{\mathrm{w}}}\right)\nabla^2 p_{\mathrm{w}}=\dfrac{\alpha}{\lambda+2G}\dfrac{\partial}{\partial t}p_{\mathrm{w}}+q_{\mathrm{w}}\end{cases}\tag{18}$$

2.5. Analytical Solutions. Before the analytical process, the relationship between the gas density and gas viscosity is derived.

In the theoretical analysis of coal mining, the volume coefficient B_α is usually introduced due to the fact that the density of ground standard state is easier to measure, ($\rho_\alpha = \rho_{\alpha\mathrm{sc}}/B_\alpha, \alpha = (\mathrm{g}, \mathrm{w})$, $\rho_{\alpha\mathrm{sc}}$ is the ground standard state density).

Firstly, the compressibility coefficient is introduced. Under isothermal conditions, the compressibility coefficient of the fluid c_{f} is expressed as

$$c_{\mathrm{f}} = -\frac{1}{V}\frac{dV}{dp} = \frac{1}{\rho}\frac{d\rho}{dp}, \quad T = \text{constant}, \tag{19}$$

where V is the volume of fluid and p is the pressure. Since the dimension of pressure is Pa or MPa, the unit of compressibility is Pa^{-1} or MPa^{-1}.

Integrating both sides of Equation (21) yields

$$\rho = \rho_{\mathrm{sc}} e^{[c_{\mathrm{f}}(p-p_{\mathrm{o}})]}, \tag{20}$$

where the density ρ_{sc} corresponds to the reference pressure p_{sc} under standard atmospheric pressure.

The expression between viscosity and pressure is as follows:

$$\mu_p = \mu_{p_{\mathrm{sc}}} e^{b(p-p_0)}, \tag{21}$$

where μ_p and $\mu_{p_{\mathrm{sc}}}$ are the viscosities under pressure p and atmospheric pressure p_{sc}, respectively. b is the pressure coefficient, which is proportional to void volume and inversely proportional to absolute temperature.

In this paper, for the convenience of distinction, the viscosities of μ_α and $\mu_{\alpha\mathrm{sc}}$ are corresponding to the pressures of p and p_{sc}, respectively, with $\alpha = (g, w)$.

Combining Equations (20) and (21) yields

$$\frac{\rho_\alpha}{\mu_\alpha} = \frac{\rho_{\alpha\mathrm{sc}}}{\mu_{\alpha\mathrm{sc}}} \cdot \frac{e^{[c_{\mathrm{f}}(p-p_{\mathrm{sc}})]}}{e^{b(p-p_{\mathrm{sc}})}}. \tag{22}$$

Taylor series expansion is carried out to $f(x) = e^x$ at $x = 0$, which yields

$$e^x = 1 + \frac{1}{1!}x + \frac{1}{2!}x^2 + \cdots + \frac{1}{n!}x^n + \cdots, x \in (-\infty, +\infty) \tag{23}$$

and

$$\begin{aligned}(\mathrm{i})\rho_\alpha &= \rho_{\alpha\mathrm{sc}} \cdot e^{[c_{\mathrm{f}}(p-p_0)]}\\ &= \rho_{\alpha\mathrm{sc}} \cdot [1 + c_{\mathrm{f}}(p - p_{\alpha 0})] + R_n(x) \to \rho_{\alpha\mathrm{sc}}\\ &\quad \cdot [1 + c_{\mathrm{f}}(p - p_{\alpha 0})]\end{aligned} \tag{24}$$

$$\begin{aligned}(\mathrm{ii})\frac{\rho_\alpha}{\mu_\alpha} &= \frac{\rho_{\alpha\mathrm{sc}}}{\mu_{\alpha\mathrm{sc}}} \cdot \frac{e^{[c_{\mathrm{f}}(p-p_{\alpha 0})]}}{e^{b(p-p_{\alpha 0})}}\\ &= \frac{\rho_{\alpha\mathrm{sc}}}{\mu_{\alpha\mathrm{sc}}} \cdot e^{[(c_{\mathrm{f}}-b)(p-p_{\alpha 0})]}\\ &= \frac{\rho_{\alpha\mathrm{sc}}}{\mu_{\alpha\mathrm{sc}}} \cdot [1 + (c_{\mathrm{f}} - b)(p - p_{\alpha 0})] + R_n(x) \to \frac{\rho_{\alpha\mathrm{sc}}}{\mu_{\alpha\mathrm{sc}}} \cdot 1,\end{aligned} \tag{25}$$

where $R_n(x) = (e^{\xi x}/(n+1)!)x^{n+1}(0 \le \xi \le 1)$, which is the Lagrange residual term of e^x, with $\lim_{n\to\infty} R_n(x) = 0$.

2.5.1. Solving Process. Figure 1 shows the schematic diagram of a single-coalbed in CBM mining process. In the single-coalbed CBM development case, both the values of q_{w} and q_{g} from model (II) are 0. Suppose the coal seam is infinite cylinder, the solution of model can be converted into the following definite problems (III) and (IV).

$$(\mathrm{III})\begin{cases}\dfrac{\partial p_{\mathrm{g}}}{\partial t} = \eta_1^2\left(\dfrac{\partial^2 p_{\mathrm{g}}}{\partial r^2} + \dfrac{1}{r}\dfrac{\partial p_{\mathrm{g}}}{\partial r}\right) \quad (0 < r < R, t > 0),\\ p_{\mathrm{g}}(r, 0) = p_0,\\ p_{\mathrm{g}}(R, t) = p_0,\end{cases}\tag{26}$$

where

$$\eta_1^2 = \frac{(kk_{\mathrm{rw}}\rho_{\mathrm{w}}/\mu_{\mathrm{w}}) + \left(R_{\mathrm{sw}}kk_{\mathrm{rg}}\rho_{\mathrm{g}}/\mu_{\mathrm{g}}\right)}{\phi\left((R_{\mathrm{sw}}s_{\mathrm{w}}\rho_{\mathrm{w}}/B_{\mathrm{w}}) + \left(s_{\mathrm{g}}\rho_{\mathrm{g}}/B_{\mathrm{g}}\right)\right) + (\alpha/(\lambda + 2G))}. \tag{27}$$

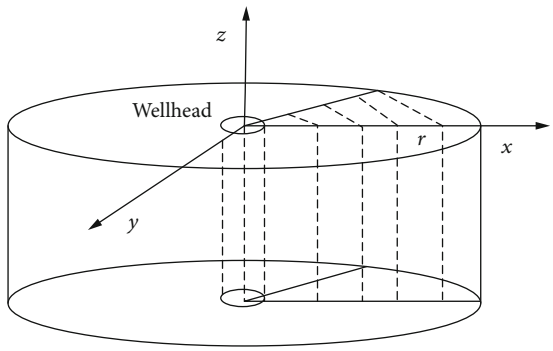

Figure 1: Schematic of development of single coal seam.

p_0 is the initial pore pressure in the coal seam, r is the distance to the center of the well, and t is the time.

$$(\mathrm{IV})\begin{cases} \dfrac{\partial p_w}{\partial t} = \eta_2^2\left(\dfrac{\partial^2 p_w}{\partial r^2} + \dfrac{1}{r}\dfrac{\partial p_w}{\partial r}\right) & (0 < r < R, t > 0), \\ p_w(r,0) = p_0 & (0 \le r \le R), \\ p_w(R,t) = p_0 & (R \to \infty), \end{cases} \tag{28}$$

where $\eta_2^2 = (kk_{rw}/\mu_w \phi s_w)((\lambda + 2G)/\alpha)$.

To simplify the calculation of definite problems (III) and (IV), a general form of definite problem (V) is constructed as

$$(\mathrm{V})\begin{cases} \dfrac{\partial p}{\partial t} = \eta^2\left(\dfrac{\partial^2 p}{\partial r^2} + \dfrac{1}{r}\dfrac{\partial p}{\partial r}\right) & (0 < r < R, t > 0), \\ p(r,0) = p_0, \\ p(R,t) = p_0 \end{cases} \tag{29}$$

Method of variable separation is used in solving problem (V) as follows.

Firstly, assuming that

$$p(r,t) = V_1(r)T_1(t). \tag{30}$$

Then, separation of variables is made after this expression generated into problem (V); after that, order

$$\frac{rV'' + V'}{rV} = \frac{T'}{\eta^2 T} = -\gamma, \tag{31}$$

$$T' + \gamma\eta^2 T = 0, \tag{32}$$

$$V'' + \frac{1}{r}V' + \gamma V = 0, \tag{33}$$

Equation (33) represents the zero-order Bessel equation. Then, eigenvalue problems will be solved as

$$\begin{cases} V'' + \dfrac{1}{r}V' + \gamma V = 0, \\ V(R) = 0 \qquad (R \to \infty), \\ |V(0)| < +\infty. \end{cases} \tag{34}$$

It should be noted that $\gamma \le 0$ is not an intrinsic value. Multiply Equation (34) with rV, and we have

$$rV''V + VV' + \gamma r V^2 = 0, \tag{35}$$

namely,

$$\gamma r V^2 = -V\left(rV'\right)'. \tag{36}$$

Integrate to both ends of Equation (36) from 0 to R, and we have

$$\gamma\int_0^R rV^2 dr = \int_0^R r\left(\frac{dV}{dr}\right)^2 dr. \tag{37}$$

If $\gamma \le 0$, then

$$\int_0^R r\left(\frac{dV}{dr}\right)^2 dr \le 0, \tag{38}$$

that is to say,

$$\frac{dV}{dr} = 0. \tag{39}$$

Hence

$$V(r) = \mathrm{C}, \tag{40}$$

where C is constant.

Nevertheless, as

$$V(R) = 0, \tag{41}$$

there must be

$$V(r) \equiv 0. \tag{42}$$

$\gamma \le 0$ is not an intrinsic value.

Making

$$\rho = \sqrt{\gamma}r. \tag{43}$$

Considering $V(\rho/\sqrt{\gamma})$ as $V(\rho)$, let us discuss the condition of $\gamma > 0$ in Equation (34), by

$$\begin{aligned} V(r) &= V_\rho \rho_r = \sqrt{\gamma} V_\rho, \\ V_{rr} &= \gamma V_{\rho\rho}, \\ \frac{1}{r} V_r &= \frac{\sqrt{\gamma}}{\rho} \sqrt{\gamma} V_\rho = \frac{\gamma}{\rho} V_\rho. \end{aligned} \tag{44}$$

We can obtain

$$V'' + \frac{1}{\rho} V' + V = 0. \tag{45}$$

The solution of Equation (45) is

$$V(r) = c_1 J_0(\rho) + c_2 N_0(\rho) = c_1 J_0(\sqrt{\gamma} r) + c_2 N_0(\sqrt{\gamma} r), \tag{46}$$

where J_0 represents zero-order Bessel function and N_0represents zero-order Neumann functions, which have the approximate expression, respectively.

$$\begin{aligned} J_0(x) &= 1 - \frac{1}{4} x^2, \\ N_0(x) &= \frac{2}{\pi} \left(\ln \frac{x}{2} + c \right), \end{aligned} \tag{47}$$

where c is Euler's constant, with a value of 0.577216. According to the natural boundary conditions, the value of c_2 is 0. And the boundary condition is

$$c_1 J_0(\sqrt{\gamma} R) = 0. \tag{48}$$

If $c_1 \neq 0$, then

$$J_0(\sqrt{\gamma} R) = 0. \tag{49}$$

Yet, the number of zero point of zero-order Bessel function can be several. Set the zero point to $\mu_m^{(0)} (m = 1, 2, \cdots)$; thus,

$$\begin{aligned} \sqrt{\gamma_m} R &= \mu_m^{(0)}, \\ \gamma_m &= \left(\frac{\mu_m^{(0)}}{R} \right)^2 (m = 1, 2, \cdots). \end{aligned} \tag{50}$$

Intrinsic function is

$$V_m = c_m J_0 \left(\frac{\mu_m^{(0)}}{R} r \right) (m = 1, 2, \cdots). \tag{51}$$

Substituting the value of γ_m into Equation (32), we have

$$\begin{aligned} T' + \left(\frac{\mu_m^{(0)} \eta}{R} \right)^2 T &= 0, \\ T_m &= D_m e^{-\left(\mu_m^{(0)} \eta / R\right)^2 t}, \\ p_m(r, t) &= A_m e^{-\left(\mu_m^{(0)} \eta / R\right)^2 t} J_0 \left(\frac{\mu_m^{(0)}}{R} r \right). \end{aligned} \tag{52}$$

To overlay p_m, the constant A_m is determined as follows:

$$\begin{aligned} p(r, t) &= \sum_{m=1}^{\infty} p_m(r, t) \\ &= \sum_{m=1}^{\infty} A_m e^{-\left(\mu_m^{(0)} \eta / R\right)^2 t} J_0 \left(\frac{\mu_m^{(0)}}{R} r \right) \\ &= \sum_{m=1}^{\infty} A_m e^{-\left(\mu_m^{(0)} \eta / R\right)^2 t} J_0 \left(\frac{\mu_m^{(0)}}{R} r \right), \end{aligned} \tag{53}$$

where

$$p(r, 0) = \sum_{m=1}^{\infty} A_m J_0 \left(\frac{\mu_m^{(0)}}{R} r \right) = p_0. \tag{54}$$

Owing to the orthogonal system with weight r constituted by $J_0((\mu_m^{(0)}/R)r)(m = 1, 2, \cdots)$,

$$\int_0^R r J_0 \left(\frac{\mu_m^{(0)}}{R} r \right) J_0 \left(\frac{\mu_m^{(0)}}{R} r \right) dr = \begin{cases} 0 & (m \neq n), \\ M_m^2 & (m = n). \end{cases} \tag{55}$$

A_m is the generalized Fourier coefficient of $p(r, 0) = p_0$, namely,

$$A_m = \frac{1}{M_m^2} \int_0^R r p(r, 0) J_0 \left(\frac{\mu_m^{(0)}}{R} r \right) dr (m = 1, 2, \cdots), \tag{56}$$

Substituting A_m into Equation (53), the solution of the definite problem (V) is

$$p(r, t) = \sum_{m=1}^{\infty} \frac{1}{M_m^2} e^{-\left(\mu_m^{(0)} \eta / R\right)^2 t} J_0 \left(\frac{\mu_m^{(0)}}{R} r \right) \int_0^R p(r, 0) J_0 \left(\frac{\mu_m^{(0)}}{R} r \right) dr, \tag{57}$$

where

$$p(r, 0) = \sum_{m=1}^{\infty} \frac{1}{M_m^2} J_0 \left(\frac{\mu_m^{(0)}}{R} r \right) \int_0^R r p(r, 0) J_0 \left(\frac{\mu_m^{(0)}}{R} r \right) dr. \tag{58}$$

Table 1: Production of methane and water in No. 3 seam of 1# test well, Shanxi.

Stage	Mining time (t, d)	Mean daily water production (v, m^3/d)	Cumulative daily water production (q, m^3)	Mean daily gas production (v, m^3/d)	Cumulative daily gas production (q, m^3)
(I) Water flow stage	120	3.95	482.1	0	0
(II) Free gas desorption	44	4.8	211.4	3398.4	146011
(III) Fluctuation desorption	129	2.96	381.8	3844.2	495907
(IV) Stable desorption	1500	0.5	750	2500	3750000
(V) Decreasing desorption	1200	0.2	240	500	600000

Substitute Equations (51) and (62) into Equation (57); hence,

$$M_m^2 = \int_0^R rJ_0\left(\frac{\mu_m^{(0)}}{R}r\right)J_0\left(\frac{\mu_m^{(0)}}{R}r\right)dr = \int_0^R r\left[1-\frac{1}{4}\left(\frac{\mu_m^{(0)}}{R}r\right)^2\right]^2\Bigg)dr. \tag{59}$$

Given $m=2$, by the definition$\mu_m^{(0)} = \pm 2$, the above equation becomes

$$M_m^2 = \int_0^R r\left[1-\frac{1}{4}\left(\frac{\mu_m^{(0)}}{R}r\right)^2\right]^2\Bigg)dr = \frac{R^2}{6}. \tag{60}$$

Substituting Equation (60) into Equation (57), the analytical solutions of definite problem (V) is

$$p(r,t) = p_0 e^{-(2\eta/R)^2 t}. \tag{61}$$

2.5.2. Final Solution. Combining Equation (61) with definite problems (III) and (IV), the solution of gas pressure at the two-phase flow stage is

$$p_g(r,t) = p_0 e^{-(2\eta_1/R)^2 t}, \tag{62}$$

where

$$\eta_1^2 = \frac{(KK_{rw}\rho_w/\mu_w) + \left(R_{sw}KK_{rg}\rho_g/\mu_g\right)}{\phi\left((R_{sw}s_w\rho_w/B_w) + \left(s_g\rho_g/B_g\right)\right) + (\alpha/(\lambda+2G))}. \tag{63}$$

The solution of water pressure at the two-phase flow stage is

$$p_w(r,t) = p_0 e^{-(2\eta_2/R)^2 t}, \tag{64}$$

where $\eta_2^2 = kk_{rw}/\mu_w\phi s_w \cdot (\lambda+2G)/\alpha$.

2.6. Model Verification

2.6.1. Field Data. The engineering data is from Jincheng 1# test well of Shanxi province, China. The No. 3 seam experiences single coal seam development, whose mineral depth is from 521.6 m to 527.4 m, the minimum horizontal stress on the main seam tested by hydraulic fracturing is 7.9 MPa~9.4 MPa, and the maximum horizontal stress determined from long spacing sonic and coal reservoir fracture pressure is 13.7 MPa~15.7 MPa. Meanwhile, the actual measured gas content is 19.6 m^3/t, and the free gas is in dynamic equilibrium with the adsorbed gas, with gas saturation 73.0%. The single-well drainage area is within $S = 0.09\,km^2$.

Table 1 describes the daily actual measured gas production and water production of different time and exploitation stages, among of which I-V represents water flow stage, free gas desorption stage, fluctuation desorption stage, stability desorption stage, and attenuation desorption stage, respectively.

Table 2 shows physical parameters of coal bed; various physical parameters will be validated with the theoretical model.

2.6.2. Verification of Theoretical Model on Fluid Pressure. As the analytical solution of the gas and water pressure has been given by Equations (62) and (64), substituting each parameter value into the theoretical model yields the gas pressure near the wellhead:

$$p_w(r,t) = 2.409e^{-3.7113\times10^{-3}t}, \quad p_g(r,t) = 2.69e^{-5.2857\times10^{-4}t}, \quad t > 120. \tag{65}$$

As shown in Figure 2, the gas pressure curve near the wellbore calculated by the theoretical model was compared with the field pressure data from No. 3 seam of 1# test well. The figure shows that water will be drained from the beginning in the mining process, while gas production occurred after the first 120 days. Firstly, both the pressure of gas and water are decreasing; secondly, the speed of the fluid decrease eventually tends to 0, and the pressure change approaches flattening. This is because as gas desorption occurs with time increasing, correspondingly, the increasing gas migration

Table 2: Physical parameters of No. 3 seam of 1# test well, Shanxi.

Parameter	Value
Young's modulus of coal (E, GPa)	2.735
Poisson's ratio of coal υ	0.25
Coal density (ρ, kg/m^3)	1500
Seam depth (h, m)	521.6
Seam thickness (H, m)	5.8
Porosity ϕ	4.29%
Permeability (K, 10^{-3} μm ^{2})	3.801
Seam initial pressure (p, MPa)	3.99
Water viscosity in the ground condition (μ_w, Pa·s)	5.8×10^{-4}
Gas viscosity under standard atmospheric pressure (μ_{gsc}, Pa·s)	1.47×10^{-5}
Gas density under standard atmospheric pressure (ρ_{gsc}, kg/m^3)	0.425
Water density under standard condition (ρ_w, kg/m^3)	998
Formation volume factor of gas B_g	0.00896
Formation volume factor of water B_w	1.0
The initial gas saturation s_g	0.73
Water saturation s_w	0.27
Solubility R_{sw}	1.3
Relative permeability of gas K_{rg}	1
Relative permeability of water K_{rw}	0.0001
Seam radius (R, m)	300

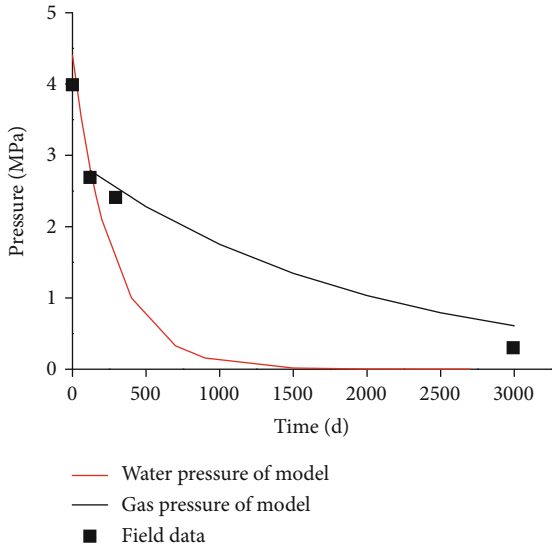

Figure 2: Variation of fluid pressure with time.

velocity results in the gas pressure drop. With the effect of desorption, the amount of desorbed gas gradually reduces, thereby leading to the drop of changing rate of gas pressure.

It is given that the original reservoir pressure is 3.99 MPa, gas pressure is 2.69 MPa, critical desorption pressure is 2.41 MPa, and the depletion pressure 0.3 MPa. The pressure obtained from this two-phase separate flow model can well fit the measured field data.

2.6.3. Verification of Theoretical Model on Gas Flow Rate. The shale gas production rate is defined as [22]

$$\frac{d\left[G_p(t)\right]}{dt} = -\int\left(\frac{\phi}{p_a}\frac{dp_g}{dt}\right)dv, \tag{66}$$

where p_a = 101.325kPa.

Based on Darcy's law, the relationship between shale gas production and water production is obtained by Xue et al. [23].

$$\frac{G_{p_g}}{G_{p_w}} = \frac{k_{rg}}{k_{rw}}\frac{\Delta p_g}{\Delta p_w}\frac{\mu_w}{\mu_g}. \tag{67}$$

Equation (67) can be transformed into the final form of water production rate as

$$\frac{d\left[G_{p_w}(t)\right]}{dt} = \frac{k_{rw}}{k_{rg}}\cdot\frac{\mu_g}{\mu_w}\cdot\frac{\Delta p_w}{\Delta p_g}\cdot\frac{d\left[G_p(t)\right]}{dt}. \tag{68}$$

Substituting each parameter of Table 2 into Equations (66) and (68) can yield the results of the water and gas production rate. Figures 3 and 4 represent the performance of the water production rate and gas production rate with time, respectively. The figure shows that in the interval of 0~120 days, the coal seam is at the single-phase fluid flow stage from the in situ data, and no gas is output at this stage; in the interval of 120~295 days, the fluid flow is at a nonsaturated stage,

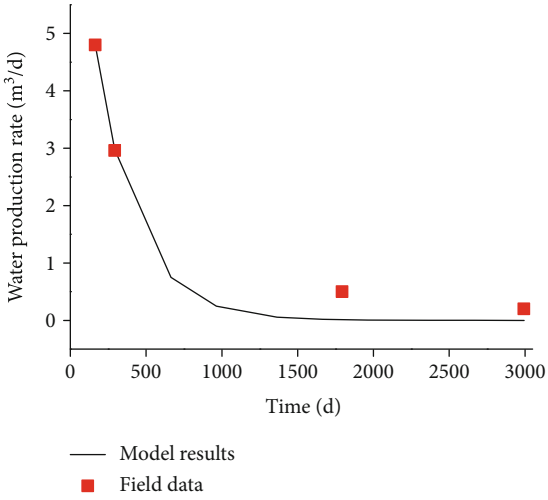

Figure 3: Variation of water production rate with time.

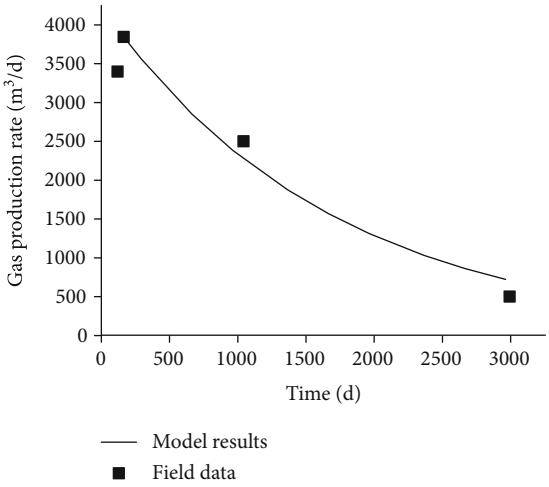

Figure 4: Variation of gas production rate with time.

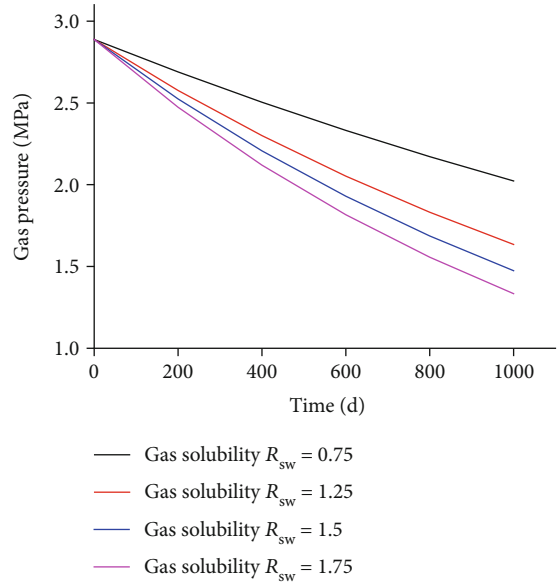

Figure 5: Effect of gas solubility on pressure change.

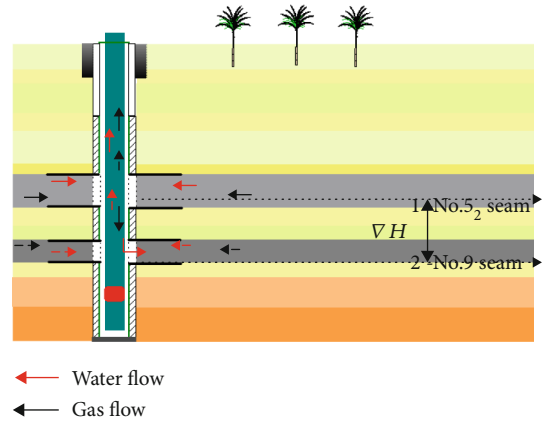

Figure 6: Schematic for multicoal seam development of TS-1 well.

and since the speed at this stage does not seek a mathematical expression, the curve is expressed by the boundary value of the single-phase fluid flow stage and two-phase flow stage; furthermore, the seam enters into a stable desorption stage after 295 days. In general, the overall change of the theoretical curve and measured value is of the same trend, such as the gas production and average water production reduce with time going on, and the rate of change slow down. It is necessary to note that the theoretical curves show the trend of the ideal state, while some factors in engineering will influence the trend of gas production rate, such as the amount of water pumped in hydraulic fracturing will affect the stability of daily gas production.

2.7. The Influence of Gas Solubility on Changes of Gas Pressure. For a more comprehensive consideration, the solubility factor is intentionally added in the model for two-phase flow. Figure 5 describes the effect of the solubility on gas pressure. As is shown in Figure 5, as the value of gas solubility in water becomes larger, the decreasing magnitude of gas pressure increases, and the scope of mining becomes wider. This is due to the fact that the greater the solubility of gas in water in depressurization process, the easier the desorption of gas, and the sooner the permeation rate of gas, thus the greater the pressure drop.

3. Gas-Water Two-Phase Separate Flow Model for Multiseam CBM Development

The case of multicoal seam development is discussed in this section. According to the pressure balance principle, due to the pressure gradient in multicoal seam development, if the pressure of the wellbore is higher than that of the coal seam, intrusion of the fluid would happen; namely, the fluid will flow into the coal seam from the wellbore; otherwise, the coal seam produces gas.

Reflected into the model proposed in this paper, as shown in Figure 6, the two-phase flow for multicoal seam development was studied. Assume that the fluid pressure of coal

Table 3: Field data of TS-1 well.

Fracturing segment	Seam number	Vertical depth (m)	Thickness (m)	Reservoir pressure (MPa)	Gas content ($m^3 \cdot t^{-1}$)	Gas saturation	Well testing permeability (mD)	Critical desorption pressure (MPa)
3	5_2	531.8	2.68	6.99	10.63	94%	0.09	5.75
	9	559.6	1.39	7.02	12.00	86%		4.50

seam 1 is greater than that of coal seam 2, namely, $p_1 > p_2$, in that way, the fluid output from coal seam 1 will flow into coal seam 2. For the modeling of fluid pressure from coal seam 1, it meets the solution of definite problems (III) and (IV); but for coal seam 2, it is equivalent for fluid flowing into the coal seam, with the flow rate

$$\begin{aligned} \Delta q_{\mathrm{w}} &= \frac{k_1}{\mu_{1\mathrm{w}}} \cdot \frac{\pi {d_1}^2}{4}(p_{1\mathrm{w}} + \rho g \nabla H - p_{2\mathrm{w}}), \\ \Delta q_{\mathrm{g}} &= \frac{k_1}{\mu_{1\mathrm{g}}} \cdot \frac{\pi {d_1}^2}{4}\left(p_{1\mathrm{g}} + \rho g \nabla H - p_{2\mathrm{g}}\right), \end{aligned} \tag{69}$$

where Δq_{w} and Δq_{g} are the strength difference of water and gas between the two coal seams, respectively. k_1 is the permeability of coal seam 1. d_1 is the diameter of the wellbore. $\mu_{1\mathrm{g}}$ and $\mu_{1\mathrm{w}}$ are the viscosities of gas and water in the coal seam 1, respectively. $p_{1\mathrm{w}}$ and $p_{1\mathrm{g}}$ are the pressures of water and gas in the coal seam 1, respectively. $p_{2\mathrm{w}}$ and $p_{2\mathrm{g}}$ are the pressures of water and gas in the coal seam 2, respectively.

3.1. Solving Process. Definite problems (VI) and (VII) of the two-phase flow in coal seam 1 are constructed as follows:

$$(\mathrm{VI}) \begin{cases} p_{\mathrm{g}t} - {\eta_1}^2 p_{\mathrm{g}rr} = 0 & (0 < r < R, t > 0), \\ p_{\mathrm{g}}|_{t=0} = p_0 & (0 \le r \le R), \\ p_{\mathrm{g}}(\mathrm{R}, t) = p_0, p_{\mathrm{g}r}\big|_{r=0} = p_{2\mathrm{g}} - \rho_{\mathrm{g}} g \nabla H - p_{1\mathrm{g}} & (R \to \infty), \end{cases} \tag{70}$$

where

$$\eta_1^2 = \frac{(kk_{r\mathrm{w}}\rho_{\mathrm{w}}/\mu_{\mathrm{w}}) + \left(R_{\mathrm{sw}} kk_{r\mathrm{g}}\rho_{\mathrm{g}}/\mu_{\mathrm{g}}\right)}{\phi\left((R_{\mathrm{sw}} s_{\mathrm{w}}\rho_{\mathrm{w}}/B_{\mathrm{w}}) + \left(s_{\mathrm{g}}\rho_{\mathrm{g}}/B_{\mathrm{g}}\right)\right) + (\alpha/(\lambda + 2G))}, \tag{71}$$

$$\Delta q_{\mathrm{g}} = k_1/\mu_1 \cdot (\pi {d_1}^2/4)(p_{2\mathrm{g}} - \rho_{\mathrm{g}} g \nabla H - p_{1\mathrm{g}})..$$

$$(\mathrm{VII}) \begin{cases} p_{\mathrm{w}t} - {\eta_1}^2 p_{\mathrm{w}rr} = 0 & (0 < r < R, t > 0), \\ p_{\mathrm{w}}|_{t=0} = p_0 & (0 \le r \le R), \\ p_{\mathrm{w}}(R, t) = p_0, p_{\mathrm{w}r}|_{r=0} = p_{2w} - \rho_{\mathrm{w}} g \nabla H - p_{1\mathrm{w}} & (R \to \infty), \end{cases} \tag{72}$$

where $\eta_2^2 = (kk_{r\mathrm{w}}/\mu_{\mathrm{w}}\phi s_{\mathrm{w}}) \cdot ((\lambda + 2G)/\alpha)$ and $\Delta q_{\mathrm{w}} = (k_1/\mu_1) \cdot (\pi {d_1}^2/4)({p_{2\mathrm{w}}}' - p_{1\mathrm{w}})$.

To simplify the calculation, the similar definite problem (VIII) with the above problems is built.

$$(\mathrm{VIII}) \begin{cases} p_t - \eta^2 p_{rr} = 0 & (0 < r < R, t > 0), \\ p|_{t=0} = p_0 & (0 \le r \le R), \\ p(\mathrm{R}, t) = p_0, p_r|_{r=0} = p_2 - \rho g \nabla H - p \end{cases} \tag{73}$$

Firstly, aiming to construct a function both meeting equation and boundary conditions, the boundary conditions will experience partial homogeneous treatment.

$$w(r, t) = p_0 + (p_2 - \rho g \nabla H) r. \tag{74}$$

Substituting Equation (61) into the original problem, the conversion of function is made as

$$p(r, t) = v(r, t) + w(r, t). \tag{75}$$

Thus, $v(r, t)$ is converted into a mixed problem as

$$(\mathrm{IX}) \begin{cases} v_t - \eta^2 v_{rr} = 0 & (0 < r < R, t > 0), \\ v|_{t=0} = -(p_2 - \rho g \nabla H) r & (0 \le r \le R), \\ p(\mathrm{R}, t) = 0, p_r|_{r=0} + p = 0. \end{cases} \tag{76}$$

Separation of variables is used to solve the above problem (IX), whose detailed solution procedure is similar to problem (VI). Eventually, the solution is

$$v(r, t) = \sum_{k=1}^{\infty} \frac{1}{M_k} \int_0^r - (p_2 - \rho g \nabla H) \xi \sin \sqrt{\lambda_k} \xi e^{-\eta^2 \lambda_k t} \sin \sqrt{\lambda_k} r, \tag{77}$$

where λ is the solution of the triangulation equation of $tgv = -(v/r)$, and eigenvalues can be obtained as

$$\lambda_k = \left(\frac{v_k}{r}\right)^2 (k = 1, 2, \cdots). \tag{78}$$

Then, the solution for the definite problem (IX) is

$$\begin{aligned} p(r, t) = {} & p_0 + (p_2 - \rho g \nabla H) r \\ & + \sum_{k=1}^{\infty} \frac{1}{M_k} \int_0^r \\ & - (p_2 - \rho g \nabla H) \xi \sin \sqrt{\lambda_k} \xi e^{-\eta^2 \lambda_k t} \sin \sqrt{\lambda_k} r. \end{aligned} \tag{79}$$

Corresponding to the solution of Equation (79), the

Table 4: Physical parameters of coal bed.

Parameter	Value
Young's modulus of coal (E, GPa)	2.735
Poisson's ratio of coal υ	0.25
Coal density (ρ, kg/m^3)	1500
Seam depth (h, m)	521.6
Seam thickness (H, m)	5.8
Porosity ϕ	3.51%
Permeability (K, mD)	0.09
Seam initial pressure (p, MPa)	6.99
Water viscosity in the ground condition (μ_w, Pa·s)	5.8×10^{-4}
Gas viscosity under standard atmospheric pressure (μ_{gsc}, Pa·s)	1.47×10^{-5}
Gas density under standard atmospheric pressure (ρ_{gsc}, kg/m^3)	0.425
Water density under standard condition (ρ_w, kg/m^3)	0.998
Formation volume factor of gas B_g	0.00896
Formation volume factor of water B_w	1.0
The initial gas saturation s_g	0.73
Water saturation s_w	0.27
Solubility R_{sw}	1.3
Relative permeability of gas K_{rg}	0.3466
Relative permeability of water K_{rw}	0.0284
Seam radius (R, m)	300

expressions of gas pressure and water pressure can be obtained, respectively.

For gas flow

$$p_g(r,t) = p_0 + \left(p_{2g} - \rho g \nabla H\right) r + \sum_{k=1}^{\infty} \frac{1}{M_k} \int_0^r - \left(p_{2g} - \rho g \nabla H\right) \xi \sin \sqrt{\lambda_k} \xi e^{-\eta_1^2 \lambda_k t} \sin \sqrt{\lambda_k} r, \tag{80}$$

where

$$\eta_1^2 = \frac{(KK_{rw}\rho_w/\mu_w) + \left(R_{sw} K K_{rg} \rho_g/\mu_g\right)}{\phi\left((R_{sw} s_w \rho_w/B_w) + \left(s_g \rho_g/B_g\right)\right) + (\alpha/(\lambda + 2G))}. \tag{81}$$

For water flow

$$p_w(r,t) = p_0 + (p_{2w} - \rho g \nabla H) r + \sum_{k=1}^{\infty} \frac{1}{M_k} \int_0^r - (p_{2w} - \rho g \nabla H) \xi \sin \sqrt{\lambda_k} \xi e^{-\eta_2^2 \lambda_k t} \sin \sqrt{\lambda_k} r, \tag{82}$$

where $\eta_2^2 = (k k_{rw}/\mu_w \phi s_w) \cdot ((\lambda + 2G)/\alpha)$.

3.2. Model Verification

3.2.1. Field Data. As Table 3 shows, the field data is from TS-1 well of Liupanshui coal mine within Tianpanjiang production area in Western Guizhou, China [10].

Table 4 shows physical parameters of coal bed, which is from the field data of No. 9 coal seam; various physical parameters will be validated with the theoretical model.

3.2.2. The Analysis of Noninterfering Coal Seam Mining. The case of noninterfering coal seam mining is discussed in this section. Firstly, each parameter value of both coal seams is given in Table 4. Take $r = 0$, that is, to research the area near wellhead. Besides, it is given that the gas desorption begins from the 80th day. Without considering the interaction between the two coal seams, combined with Equations (62) and (64), the pressure of the two-phase flow can be simplified into

$$\begin{aligned} p_{1g} &= 6.348 e^{-9.6733 \times 10^{-6} t} (t > 80), \\ &\frac{n!}{r!(n-r)!} \\ p_{1w} &= 6.348 e^{-3.0915 \times 10^{-4} t} (t > 80), \\ p_{2g} &= 4.968 e^{-1.0545 \times 10^{-5} t} (t > 80), \\ p_{2w} &= 4.968 e^{-7.2133 \times 10^{-4} t} (t > 80), , \end{aligned} \tag{83}$$

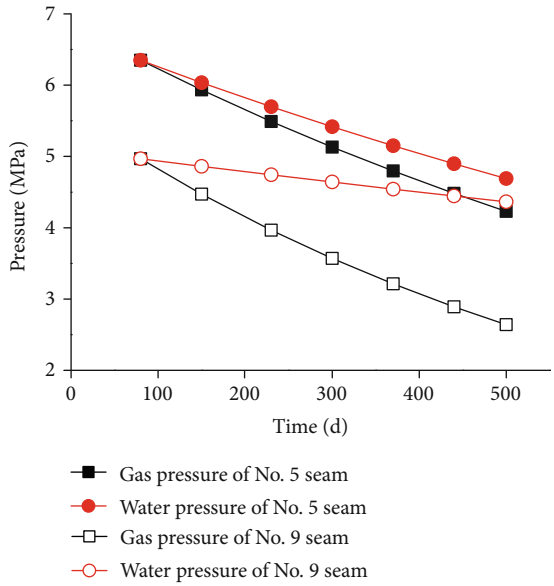

Figure 7: Fluid pressure changes of two coal seams in single coal seam mining.

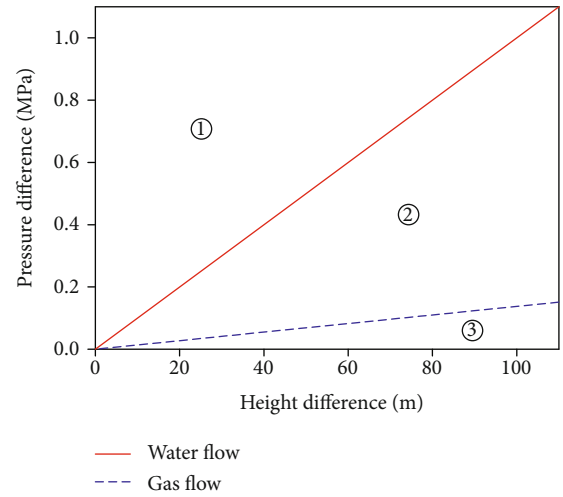

Figure 8: Relationship of pressure difference and height difference between the two coal seams.

where the subscript 1g represents gas phase of No. 5_2 seam, the subscript 1w represents water phase of No. 5_2 seam, the subscript 2g represents gas phase of No. 9 seam, and the subscript 2w represents water phase of No. 9 seam.

Figure 7 shows gas and water pressure curves of both the No. 5_2 seam and No. 9 seam in single coal seam mining. The four curves are given by the analytical solution above. As is shown in the figure, firstly, whatever the coal seam is, the gas pressure is always decreasing from the start of gas production, and the gas pressure of No. 5_2 seam is always greater than that of No. 9 seam; secondly, the solution of water pressure of both coal seams in the fluctuation desorption stage is not studied. For No. 5_2 seam, we can find that the water pressure is not always making the same trend during different water flow stages. And finally, in the 500th day, the water pressure of No. 5_2 seam drops to 4.75 MPa. In addition, for No. 9 seam, the water pressure maintains the downward trend, and the water pressure of No. 9 seam drops to 4.39 MPa in the 500th day.

3.2.3. The Effects of Factors on the Development of Multicoal Seam. The effects of factors on the development of multicoal seam are discussed in this section. The impact of altitude difference between the two coal seams is considered, and the remaining factors were not considered temporarily.

Due to the two-phase flow phenomenon in the CBM process, it should be emphasized that the two coal seams interact each other and intrusion of the fluid occurs between the two coal seams in multicoal seam development in the case that

(1) If

$$p_2 - \rho g \nabla H > p_1, \tag{84}$$

the fluid of No. 9 coal seam flows to the wellhead; meanwhile, a portion of the fluid flows backward into No. 5_2 coal seam.

(2) If

$$p_1 + \rho g \nabla H > p_2, \tag{85}$$

a portion of the fluid of No. 5_2 coal seam will not flow to the wellhead but flows vertically downward and backward into the No. 9 coal seam.

Figure 8 demonstrates the relationship of pressure difference and height difference of the two seams, both of which are the key factors to influence the development of multicoal seam. As is shown, for water flow, the red solid line represents that there are no influence of water flow between the two coal seams; namely, both the No. 9 seam and No. 5_2 seam produce water separately and have no effect on the other coal seam. In region ①, water flows from No. 9 seam into No. 5_2 seam; however, in region ②+③, gas and water from No. 5_2 seam would flow into No. 9 seam in the mining process. For gas flow, the blue dotted line means that there is no influence of gas flow between the two coal seams. In region ①+②, gas flows from No. 9 seam into No. 5_2 seam; however, gas would flow from No. 5_2 seam into No. 9 seam in region ③.

As Figures 7 and 8 show, the fluid pressure of No. 5_2 seam is always greater than that of No. 9 seam. By calculation of Equations (78)–(81), it can be obtained that the relationship of the pressure satisfies Equation (85), which means a part of the gas and water would flow backward into the No. 9 coal seam in the mining process.

3.2.4. The Analysis of Multicoal Seam Mining. As Figure 6 shows, the field data is from TS-1 well of Liupanshui coal mine; a portion of the fluid (gas and water) of No. 5_2 coal seam will not flow to the wellhead but flows vertically downward and backward into the No. 9 coal seam.

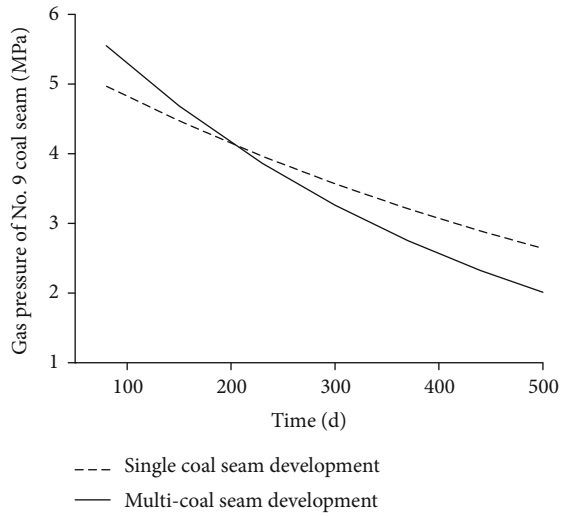

Figure 9: Effect of multicoal seam development on gas pressure.

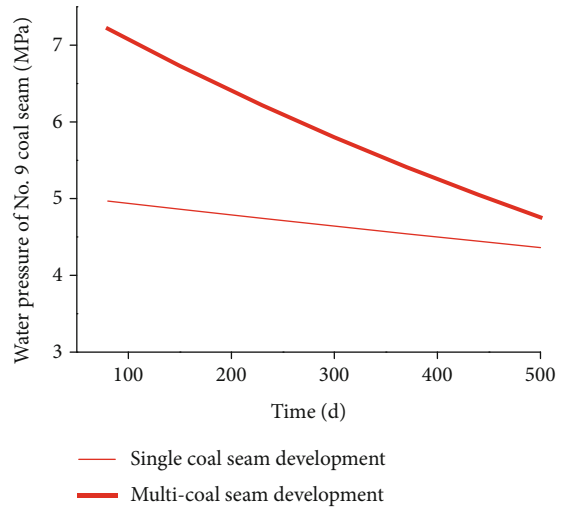

Figure 10: Effect of multicoal seam development on water pressure.

Substituting the parameter value of Tables 3and 4 into Equation (80), the expressions of the gas flow can be given as

$$p(t) = 1.104(p_0 + p_2 - \rho g \nabla H - p_1)e^{-(2.4048\eta/R)^2 t}. \quad (86)$$

Plotting according to expression from Equation (86), the contrast curves between the development of single coal seam and multicoal seam can be obtained as follows.

As Figure 9 shows, the gas pressure decreases with time regardless of whether there is interaction between the two coal seams. In addition, the gas pressure for the development of multicoal seam decreases faster than that of single coal seam. What is more, the gas pressure for the development of multicoal seam keeps higher than that of single coal seam until the 200th day, and it is lower after the 200th day. It is because when the intrusion happens, the pressure gradient increases, which can accelerate the gas production, followed by the gas pressure dropping faster.

For water phase, the classification discussion will be used as follows: when $t \le 632$ d, the pressure of No. 5_2 is greater than that of No. 9 coal seam, and the water intrusion occurs from No. 5_2 to No. 9 seam; and when $t > 632$ d, water intrusion will happen from the No. 9 to No. 5_2 seam, which does not match the time scope of $t \in (0\,\text{d}, 500\,\text{d})$ in this paper.

Thus, substituting the parameter values of Tables 3 and 4 into Equation (82), the expressions of the water flow can be given as follows:

For water flow of No. 5_2 seam

$$p_{1w} = 6.348e^{-3.0915\times10^{-4}t} 80 < t < 500. \quad (87)$$

For water flow of No. 9 seam

$$p'_{2w} = 6.348e^{-1.0305\times10^{-3}t} + 0.865467e^{-7.2133\times10^{-4}t} 80 < t < 500. \quad (88)$$

According to Equations (87) and (88), the contrast curves of water pressure between the development of single coal seam and multicoal seam can be obtained as follows.

As Figure 10 shows, the water pressure decreases with time regardless of whether there is interaction between the two coal seams. In addition, at the two-phase flow stage, the water pressure for the development of multicoal seam decreases faster. What is more, the gas pressure for the development of multicoal seam keeps lower than that of single coal seam in the whole mining of 500 days. It is because a large amount of drainage occurs in single water flow stage, and plenty of water intrusion will affect the drainage of No. 9 coal seam while considering the impact of multicoal seam; however, the amount of drainage is relatively small when the intrusion happens, and the water pressure gradient will increase in No. 9 coal seam, which can accelerate the drainage, followed by the water pressure dropping faster.

4. Conclusions

Two models of two-phase flow for the development of single coal seam layer and multicoal seam layers were developed, respectively, to simulate the fluid flow in coal seam gas reservoirs in the mining process. These models were then analytically solved by separation of variables and applied to analyze the field data from different CBM formations (the 1# test well of Jincheng and the TS-1 well of Liupanshui coal mine, China). The effects of gas solubility on the gas pressure were investigated. Besides, the impact of interlayer difference on the development of multicoal seam layers was explored. Based on these studies, the following conclusions can be made.

Firstly, the two-phase models for the development of single coal seam and multicoal seam, respectively, are proved to be correct after matching the field data well, respectively. Moreover, the gas pressure is influenced by the gas solubility; if the value of gas solubility increases, the gas pressure will drop increasingly.

Secondly, the key factors incorporating the height difference and the pressure difference of the two seams are proved to influence the multicoal seam development comprehensively. For the field from the TS-1 well of Liupanshui coal mine, during the seal layer mining process, the pressure of the upper No. 5_2 seam is greater than that of the lower No. 9 seam; thus, the gas and water will intrude into the No. 9 coal seam and stimulate the production and overall shorten the mining time.

Nomenclature

R_{sw}: Gas solubility in water
s_w: Saturations of water
ρ_w: Density of water
s_g: Saturations of gas
ρ_g: Density of gas
ρ_{gsc}: Density of gas under standard atmospheric pressure
V_w: Velocity of water
V_g: The velocity of gas
q_w: Fluid strength of water
q_g: Fluid strength of gas
∇: Hamiltonian operator
V_s: Velocity of the coal solid
k: Absolute permeability of porous media
k_{rw}: Relative permeability of water
k_{rg}: Relative permeability of gas
μ_w: Viscosity of water
μ_g: Viscosity of gas
μ_{gsc}: Viscosity of gas under standard atmospheric pressure
p_w: Pore pressure of water
p_g: Pore pressure of gas
g: Gravity acceleration
H: Vertical elevation
θ: Volumetric strain of the coal solid
σ_{ij}: Total stress tensor
f_i: Body force tensor
σ_{ij}': Effective stress tensor
p: Pore pressure of coalbed
δ_{ij}: Kronecker function
ε_{ij}: Strain tensor
α: Biot coefficient
G: Shear modulus of elasticity
λ: Lame constant
E: Modulus of elasticity
v: Poisson's ratio
u_i: Displacement component in x-direction
u_j: Displacement component in y-direction
$\mathbf{u}$: Displacement vector
p_0: Initial pore pressure in the coal seam
r: Distance to the center of the well
t: Time
J_0: Zero-order Bessel function
N_0: Zero-order Neumann functions
c: Euler's constant
A_m: Generalized Fourier coefficient.

Data Availability

The data used to support the findings of this study are available from the corresponding author upon request.

Conflicts of Interest

The authors declare that there is no conflict of interest regarding the publication of this paper.

Acknowledgments

The authors are supported by the Independent Innovation Project of "Double First Rate" of China University of Mining and Technology (Grant No. 2018ZZCX04) and the National Natural Science Foundation of China (Grant Nos. 42030810, 51934007).

References

[1] G. B. Li and G. F. Li, "Study on the differences and main controlling factors of the coal-bed methane wells between single layer and multi-layer drainage," *Journal of China Coal Society*, vol. 37, no. 8, pp. 1354–1358, 2012.

[2] US Department of Energy, *Multi-seam well completion technology: implication for Powder River Basin coalbed methane production*, National Energy Technology Laboratory, 2003.

[3] Z. Zhang, Y. Qin, J. P. Bai, X. H. Fu, and D. H. Liu, "Evaluation of favorable regions for multi-seam coalbed methane joint exploitation based on a fuzzy model:a case study in southern Qinshui Basin China," *Energy Exploration & Exploitation*, vol. 34, no. 3, pp. 400–417, 2016.

[4] X. H. Fu, Y. Y. Ge, W. Q. Liang, and S. Li, "Pressure control and fluid effect of progressive drainage of multiple superposed CBM systems," *Natural Gas Industry*, vol. 33, no. 11, pp. 35–39, 2013.

[5] S. Li, D. Z. Tang, Z. J. Pan, H. Xu, and L. L. Guo, "Evaluation of coalbed methane potential of different reservoirs in western Guizhou and eastern Yunnan, China," *Fuel*, vol. 139, pp. 257–267, 2015.

[6] Y. D. Cai, D. M. Liu, and Y. B. Yao, "Geological controls on prediction of coalbed methane of No. 3 coal seam in southern Qinshui basin, North China," *International Journal of Coal Geology*, vol. 88, no. 2-3, pp. 101–112, 2011.

[7] H. H. Liu, S. X. Sang, and G. G. Wang, "Evaluation of the synergetic gas-enrichment and higher-permeability regions for coalbed methane recovery with a fuzzy model," *Energy*, vol. 39, no. 1, pp. 426–439, 2012.

[8] Y. M. Lv, D. Z. Tang, and H. Xu, "Production characteristics and the key factors in high-rank coalbed methane fields: a case study on the Fanzhuang Block, Southern Qinshui Basin, China," *International Journal of Coal Geology*, vol. 96-97, pp. 93–108, 2012.

[9] B. Wang, F. J. Sun, and D. Z. Tang, "Hydrological control rule on coalbed methane enrichment and high yield in FZ Block of Qinshui Basin," *Fuel*, vol. 140, pp. 568–577, 2015.

[10] Z. Xiaozhi, S. Shuxun, Y. Tongsheng, J. Jun, H. Huazhou, and H. Dengcai, "Damage mechanism of upper exposed producing layers during CBM multi-coal seam development," *Natural Gas Industry*, vol. 36, no. 6, pp. 52–59, 2016.

[11] L. Y. Zhang, K. Z. Deng, and C. G. Zhu, "Analysis of stability of coal pillars with multi-coal seam strip mining," *Transactions of Nonferrous Metals of China*, vol. 21, pp. 549–555, 2011.

[12] X. H. Fu, K. Jian, Y. M. Ding, and K. X. Wang, *Gas content simulation of three-phase state in low rank coal reservoir*, Science Press, Beijing, China, 2015.

[13] C. R. Clarkson and F. Qanbari, "A semi-analytical method for forecasting wells completed in low permeability, undersaturated CBM reservoirs," *Journal of Natural Gas Science and Engineering*, vol. 30, pp. 19–27, 2016.

[14] F. I. Ahmed and A. N. Hisham, "A comprehensive model to history match and predict gas/water production from coal seams," *International Journal of Coal Geology*, vol. 146, pp. 79–90, 2015.

[15] S. A. Mahoney, T. E. Rufford, V. Rudolph, K. Y. Liu, S. Rodrigues, and K. M. Steel, "Creation of microchannels in Bowen Basin coals using UV laser and reactive ion etching," *International Journal of Coal Geology*, vol. 144-145, pp. 48–57, 2016.

[16] C. R. Clarkson and J. M. McGovern, "Optimization of CBM reservoir exploration and development strategies through integration of simulation and economics," *SPE Reservoir Evaluation and Engineering*, vol. 8, no. 6, pp. 502–519, 2005.

[17] A. S. Ziarani, R. Aguilera, and C. R. Clarkson, "Investigating the effect of sorption time on coalbed methane recovery through numerical simulation," *Fuel*, vol. 90, no. 7, pp. 2428–2444, 2011.

[18] X. H. Fu, Y. Qin, and W. G. Wang, "Study of gas-dissolving in coalbed water and prediction of gas content of lignite reservoir," *Natural Gas Geoscience*, vol. 16, no. 2, pp. 153–156, 2005.

[19] A. Liu, X. Fu, and K. Wang, "Investigation of coalbed methane potential in low-rank coal reservoirs - free and soluble gas contents," *Fuel*, vol. 11, no. 2, pp. 14–22, 2013.

[20] X. H. Fu, Y. Qin, and Y. G. Yang, "Experimental study on coalbed methane solubility in water," *Natural Gas Geoscience*, vol. 14, no. 4, pp. 345–348, 2004.

[21] K. M. Sun, B. Lang, and Y. M. Zhu, "Study of fluid-solid coupling of coal methane considered about desorption and diffusing process," *Journal of Liaoning Technical University (Natural Science)*, vol. 20, no. 4, pp. 548-549, 2001.

[22] Z. W. Chen, J. S. Liu, A. Kabir, J. G. Wang, and Z. J. Pan, "Impact of various parameters on the production of coalbed methane," *SPE Journal*, vol. 18, no. 5, pp. 910–923, 2013.

[23] Y. C. Xue, X. J. Zhang, and G. Y. Ding, "Mathematical model study on gas and water two-phase of early-time flowback in shale gas wells," *Science Technology and Engineering*, vol. 17, no. 24, pp. 213–217, 2017.